Proceedings of the 3rd GCC International Conference on Industrial Engineering and Operations Management
Tabuk, Saudi Arabia, February 2-4, 2026

Proceedings of the International Conference on Industrial Engineering and Operations Management

Publisher: IEOM Society International, USA DOI: 10.46254/GC03.20250279
Published: February 2, 2026

Impact of Post Weld Heat Treatment on Structural and Mechanical Properties of Dissimilar High Strength Steels

Lerato Shoke
Defense and Security (Landward Sciences)
Council of Scientific and Industrial Research (CSIR)
Pretoria, South Africa
Lshoke@csir.co.za

Kalenda Mutombo
Advanced Materials and Manufacturing
Council of Scientific and Industrial Research (CSIR)
Pretoria, South Africa
Kmutombo@csir.co.za

Peter Olubambi
School of Mining, Metallurgy and Chemical Engineering
University of Johannesburg
Johannesburg, South Africa
Polubambi@uj.ac.za

Mthobisi Clyde Zondi
Sandock Austral,
Johannesburg, South Africa
zondi@outlook.com

Abstract

This study explores the influence of Submerged Arc Welding (SAW) parameters on the microstructural evolution, mechanical properties, and residual stresses in dissimilar welds of A516 Gr70 and A106 GrB high-strength carbon steels. Through a comprehensive experimental approach, this study delineates the direct relationship between the welding heat input, determined by the voltage, current, and speed, and its profound impact on the heat-affected zone (HAZ) size, microstructure, and mechanical properties, such as hardness and tensile strength. The investigation revealed that the optimal welding parameters play a critical role in controlling the bead geometry and HAZ size, which in turn significantly affect the mechanical integrity and performance of the welded joint. Notably, this study revealed that a higher heat input does not necessarily lead to a larger HAZ, challenging the conventional assumptions in welding practices. Furthermore, this study delves into the effects of post-weld heat treatment (PWHT) techniques, including normalizing, quenching, and annealing, on reversing the microstructural alterations induced by welding and restoring the initial mechanical properties of the base metals. Microstructural analyses employing stereo microscopy, optical microscopy, scanning electron microscopy, and X-ray diffraction techniques provide insight into the granular details of the morphological changes across different regions of the weld, highlighting the formation of martensitic lathes in the weld bead region and variations in the pearlite-ferrite matrix. Mechanical testing and hardness profiles substantiate these findings, illustrating the significant influence of cooling rates and heat treatment methods on the mechanical properties of the weldments. This study highlights the importance of controlled heat treatment in enhancing material performance, suggesting avenues for further research into parameter optimization, fatigue assessments, and advanced heat treatment techniques to refine welding processes for industrial applications.

Keywords
Submerged Arc Welding, Dissimilar Steels, A516 Gr70, A106 GrB, Microstructure, Mechanical Properties, Post-Weld Heat Treatment, Residual Stresses, Heat-Affected Zone.

1. Introduction
Steel is indispensable in various industries, particularly in the fabrication of pressure vessels, owing to its favorable combination of manufacturability and cost-effectiveness (e.g., through microalloying and optimized rolling strategies). Modern pressure vessel steels, such as those based on ASTM A516 Gr 70, are engineered to meet stringent toughness and strength requirements. (J. Gottlieb, 2010). Among the numerous steel grades available, A516 Gr 70 and A106 Gr B are frequently chosen for pressure vessel applications because of their tailored mechanical and metallurgical properties. The selection of a steel grade for pressure vessels must consider several critical factors: the material strength under service conditions (including fracture toughness and ductility), vessel diameter (which influences stress distribution), resistance to corrosion in the service environment, and efficiency of welded joints (which affects the effective strength of the structure).

A516 Gr 70, studies have demonstrated its fracture behavior (e.g., ductile crack initiation characterized by J_{1C}) and sensitivity to orientation relative to the rolling direction. (G. de Castro Coêlho, 2023). The influence of the loading rate on toughness was also investigated, confirming the suitability of the material for pressure vessel service in moderate to low temperature conditions. (S. Sharma, 2020). (M. Daavaria, 2016) documented the mechanical and electrochemical behaviour of A106 Gr B in welded joints. For example, butt-welded A106 Gr B exhibits microstructural and electrochemical characteristics under service environments, which influence the reliability of pressure piping and vessel systems. Its corrosion behavior in sulfate environments has also been studied, revealing dependencies on ion concentration and temperature. (R. Abdel-Karim, 2018). Additionally, A106 Gr B in Na_2SO_4 media exhibited increased corrosion rates with temperature and sulfate concentration, indicating that environmental control or protective measures are crucial for long-term service. Moreover, the corrosion performance of welded A106 Gr B pipes (e.g. under different welding currents) has been correlated with microstructure changes and flow conditions (T. Yingsamphancharoen, 2016).

Regarding joint efficiencies, filler metal selection and weld impact toughness are key factors in pressure vessel design. For instance, in A516 Gr 70 fabrications, the filler metal is chosen to achieve a minimum impact toughness (e.g., ≥ 20 ft-lb at −20 °F) so as not to degrade joint performance.

More broadly, the rationale for using steel in pressure vessels is that its properties (particularly when microalloyed or heat-treated) can be optimized to balance strength, toughness, and cost, making it highly competitive among structural materials.

The welding of steel plate ASTM A516 and steel pipe ASTM A106 GrB during the manufacturing of pressure vessels using the semi-automated welding (SAW) technique induces residual stress in the nozzle-shell weld. Therefore, this study focuses on post-weld heat treatment techniques to alleviate the induced welding residual stress (WRS) on nozzle-shell welds in pressure vessel structures. Moradi & Salehebrahimnejad (2017) showed that applying PWHT to A106 GrB welds reduced residual stresses (measured via hole-drilling and FEM) by up to ~ 60 % in the welding and HAZ areas (M. Moradi, 2017).

Welding A516 Gr70 and A106 GrB steels, which are commonly employed in the fabrication of industrial boilers and pressure vessels for the oil, gas, and petrochemical sectors, introduces critical challenges that impact their operational performance and reliability. Specifically, the formation of weld defects, such as embrittlement, cracking, and increased Welding Residual Stresses (WRS), during the welding process significantly compromises the structural integrity of these components. The presence of such defects not only predisposes welded structures to premature failure but also acts as stress concentrators, exacerbating the impact of operational loads and conditions. This vulnerability is particularly concerning given the critical applications of A516 Gr70 and A106 GrB in environments subjected to extreme pressures and temperatures, where material failure can have catastrophic consequences for both safety and production continuity. Oliveira et al. (2009) investigated multipass welding on A516 Gr70 and observed elevated residual stresses, especially in the weld root, with accompanying microhardness peaks, emphasizing the influence of weld passes and heat input on the WRS and microstructure. (De & D. Silva, 2009)

Moreover, the induction of WRS and defects during welding poses a direct challenge to adhering to stringent industry standards and safety regulations, such as those outlined in the ASME Boiler and Pressure Vessel Code. These standards require a meticulous balance between mechanical properties, such as tensile strength, toughness, and ductility, which are altered by the localized thermal cycles induced by welding. However, current standards and protocols for welding the nozzle shell are not clearly defined, indicating a need for comprehensive data to inform best practices and regulatory updates.

Welding affects a material's ability to withstand operational stresses without succumbing to failure. The alteration in the microstructure within the heat-affected zone (HAZ) and fusion zone during welding further complicates the attainment of the desired mechanical properties, necessitating sophisticated post-weld heat treatment (PWHT) techniques to restore material homogeneity and alleviate induced stresses. Wang et al. (2024) used post-weld annealing on SA516 Gr70 joints made by SMAW and FSW, finding significant improvements in toughness and ductility in the HAZ due to microstructural refinement and reduction of hard phases through annealing, demonstrating efficacy of PWHT techniques. (X. Wang, 2024)

Given the pivotal role of A516 Gr70 and A106 GrB steels in the fabrication of pressure vessels and their susceptibility to weld-induced defects, comprehensive research aimed at optimizing welding parameters and post-weld treatments is critical. Such advancements are essential for enhancing the performance and safety of welded components, ensuring compliance with industry standards, and ultimately safeguarding the reliability of critical infrastructure in the oil, gas, and petrochemical industries.

1.1 Objectives

The specific objectives of this study are as follows:

i. To determine the optimal welding parameters (voltage, current, and welding speed) that minimize the heat-affected zone (HAZ) and welding residual stresses in dissimilar high-strength carbon steels welded using the submerged arc welding (SAW) method.
ii. To analyze the microstructural transformations in the weld zone and HAZ of welded specimens under various welding parameters to identify the formation of critical phases affecting mechanical properties.
iii. To evaluate the effectiveness of different PWHT techniques (normalizing, quenching, and annealing) at specified temperatures (950°C and 1050°C) in homogenizing the microstructure and relieving WRS without altering the initial mechanical properties of the base materials.
iv. To conduct mechanical testing (hardness and tensile strength) on both as-welded and post-weld heat-treated specimens to assess the influence of welding parameters and heat treatment on the mechanical integrity of the weldments.

2. Literature Review

Pressure vessels are closed systems designed to contain fluids and gases at elevated pressures and temperatures. They are widely used in the petrochemical, power generation, and chemical processing industries, among others. Typical pressure vessels consist of cylindrical or spherical shells fitted with nozzles, heads, flanges, and internals that are assembled primarily through welding. Design, fabrication, and inspection are governed by international standards, such as the ASME Boiler and Pressure Vessel Code, to ensure structural integrity and safe operation (ASME, 2015; Tirenti, 2024).

The material selection for pressure vessel applications is governed by the strength, fracture toughness, weldability, and performance under service temperatures and pressures. Carbon steels, such as ASTM A516 Grade 70, are commonly used for pressure vessel shells because of their favorable combination of strength, ductility, and toughness over operating temperatures ranging from −29 °C to 427 °C (Akademia Baru et al., 2016). ASTM A106 Grade B carbon–manganese steel is widely employed for pressure piping and nozzles in high-temperature and high-pressure environments, particularly in oil and gas and power-generation applications. Therefore, dissimilar welding between these steels is common in nozzle-to-shell configurations.

Submerged arc welding (SAW) is frequently employed in pressure vessel fabrication because of its high deposition rate, deep penetration capability, and suitability for thick-section welding (Croft, 1989; Kou, 2002). Welding parameters, such as current, voltage, travel speed, and wire feed rate, directly influence the heat input, which governs the weld bead geometry, microstructural evolution, and extent of the heat-affected zone (HAZ) (Suryana et al., 2019). The thermal cycles associated with welding produce heterogeneous microstructures across the weld metal, HAZ, and base material, leading to nonuniform mechanical properties.

Welding-induced residual stresses (WRS) arise from steep thermal gradients, constrained thermal contraction, and solid-state phase transformations during cooling. In ferritic steels, phase transformations between austenite and ferrite or martensite play a critical role in the development of residual stress owing to the associated volumetric changes (Deng, 2009). Experimental and numerical studies have shown that the residual stresses in welded joints significantly influence the fatigue life, crack initiation, and crack propagation behavior, particularly in pressure vessel components subjected to cyclic loading (Lu, 2002; Rossini et al., 2014). Tensile residual stresses are generally detrimental, whereas compressive residual stresses may improve fatigue resistance, depending on their magnitude and distribution.

Nozzle-to-shell welds are particularly susceptible to high residual stress concentrations owing to geometric discontinuities and multiaxial stress states. Failure analyses of pressure vessels frequently identify the HAZ as the critical failure location, particularly in ferritic steels (Akbari and Sattari-Far, 2009). Weld defects such as lack of penetration, slag inclusions, and excessive reinforcement further exacerbate stress concentrations and reduce fatigue resistance.

Post-weld heat treatment (PWHT) is commonly applied to relieve residual stresses and homogenize microstructures in welded pressure vessel components. PWHT has been shown to significantly reduce residual stresses in carbon steel welds, although prolonged exposure or elevated treatment temperatures may lead to strength degradation due to carbide coarsening or cementite decomposition, particularly in high-carbon steels (Qin et al., 2018). Therefore, the effectiveness of PWHT is dependent on the material composition, treatment temperature, and cooling conditions.

Despite extensive studies on welding residual stresses and PWHT in pressure vessel steels, limited experimental data are available for dissimilar nozzle-to-shell welds produced by SAW, particularly regarding the combined effects of welding parameters, microstructural evolution, and residual stress distributions. This study addresses this gap by systematically investigating the influence of the SAW parameters and post-weld heat treatment on the microstructure, mechanical properties, and residual stresses of dissimilar welded joints of ASTM A516 Grade 70 and ASTM A106 Grade B steels.

3. Methodology

A 10 mm thick as-received ASTM A516 Grade 70 steel plate was waterjet-cut to 178 mm × 178 mm and machined to create an 80 mm diameter central opening for nozzle integration (Figure 1). An as-received ASTM A106 Grade B pipe (80 mm diameter) was subsequently welded to the plate to form a nozzle-to-shell configuration. The welding process employed a three-pass submerged arc welding (SAW) technique using at an ambient laboratory temperature.

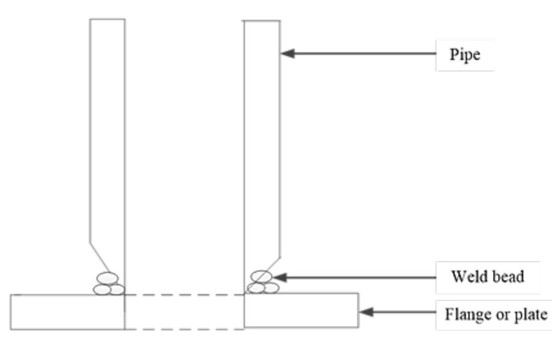

Figure 1. Schematic diagram of as-received ASTM A516 Grade 70 steel plate welded to ASTM A106 Grade B pipe

Welding was performed without preheating or post-weld heat treatment, and the specimens were allowed to cool naturally to room temperature. The welding parameters, specifically current, voltage, travel speed, and wire feed rate, were systematically varied according to the experimental matrix presented in Table 1, covering a range of heat inputs. Each welding pass used distinct parameters as detailed in the table.

Table 1. Input Parameters

Input Parameters					
	I (Amp)	**V (Volts)**	**S (mm/s)**	**FR (mm/s)**	**Mode**
S4	380	30	10	18.3	CA
S6	380	25	8	18.3	CA
S7	360	25	8	18.3	CA
S8	360	25	10	18.3	CA
S9	380	25	10	18.3	CA
S12	360	30	8	16.7	CW
S13	360	30	8	18.3	CW
S15	360	25	8	18.3	CW
S16	360	25	8	16.7	CW

For microstructural characterization, L-shaped specimens were sectioned using waterjet cutting from the welded joints, ensuring representation of the base metal, HAZ, and weld metal (Figure 2a). These specimens were then hot-mounted in Bakelite resin, ground using SiC papers (P240, P600, P1200, P2400 grits), and polished with diamond suspensions (6 µm, 3 µm, 1 µm) to a mirror finish. Etching was performed using a 2–5% Nital solution for 10–15 seconds to reveal microstructural features. Phase analysis was conducted using X-ray diffraction (XRD) with a diffractometer employing Cu-Kα radiation (λ = 1.5406 Å) at 40 kV and 40 mA. Scans were performed from 2θ = 20° to 100° with a step size of 0.02° and a dwell time of 1 second per step. Microstructural characterization of the as-received, as-welded, and post-weld heat-treated specimens was performed using an optical microscope and a scanning electron microscope operated at 15 kV.

Micro-Vickers hardness testing was conducted using a micro-indenter with a load of 300 gf and a dwell time of 15 seconds. Hardness profiles were measured across the pipe, weld metal, and flange regions, traversing the base metal, HAZ, and weld metal with a consistent indentation spacing. A minimum of 5 indentations were made per region to ensure statistical validity. Additional hardness measurements (average of 10 indentations) were performed on the as-received plate and pipe specimens. The yield strength and ultimate tensile strength were estimated from the hardness values using the empirical correlations proposed by Pavlina and Van Tyne:

$$YS = -90.7 + 2.876H_v \text{ ----------------------- } (1)$$

$$UTS = -99.8 + 3.73H_v \text{ ----------------------- } (2)$$

Residual stresses were measured using neutron diffraction (ND). A stress-free reference lattice spacing was obtained using L-shaped reference specimens. Measurements were conducted at 3 mm intervals along the flange and pipe directions of the specimen. The strain was measured in the radial, hoop, and axial directions using specimen reorientation. Measurements were performed using the MPISI neutron strain scanner with a 2 mm collimator and 2 mm × 2 mm slit, defining an 8 mm³ gauge volume. The gauge volume was positioned at mid-thickness and at least 1.6 mm below the surface of the specimen.

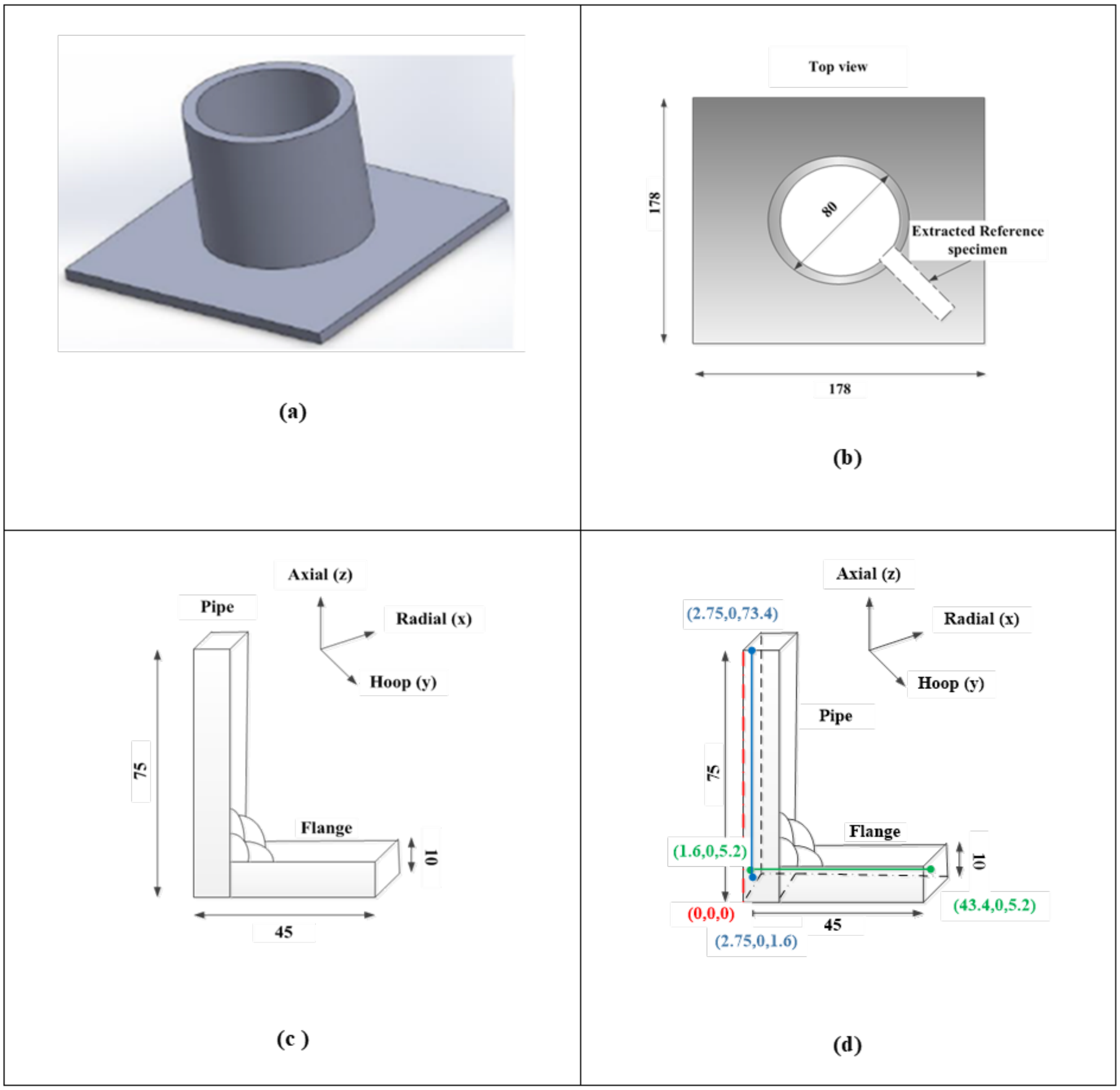

Figure 1. a) Schematic illustration of a top view of the welded component and the area where the L-shaped reference specimen was sectioned. (b), (c) Below the top view is a 3D CAD image of the welded component (d) Post-weld heat treatment was performed on six L-shaped specimens from each welded component at 950 and 1050 °C, followed by air cooling, furnace cooling, or water quenching.

4. Results and Discussion

4.1 Bead Geometry, Heat Input, and HAZ Development

Figure 3 presents a macrograph of a sectioned L-shaped specimen, revealing the distinct regions of the pipe, HAZ, weld bead, and plate. The black circular area is the Bakelite resin, and the grey area is an image of the sectioned specimen. Macroscopic examination confirmed sound weld formation across all samples, with clearly defined boundaries between the plate, weld metal, and pipe regions. The bead geometry varied systematically with welding parameters, reflecting changes in heat input (HI).

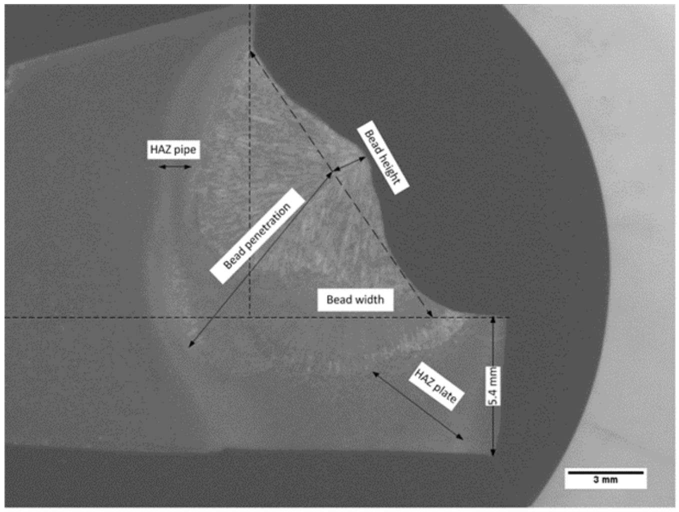

Figure 2. A stereo macrograph showing a sample sectioned from the welded specimen

The effect of HI is quantified by the size of the HAZ. Figure 4 quantifies the effect of heat input (HI) on HAZ size, presenting calculated HI values against measured HAZ dimensions for both the pipe and plate regions. While higher HI generally increased bead width and penetration, the relationship between HI and HAZ size was not strictly linear. Notably, samples with identical HI but varying feed or travel rates showed markedly different HAZ dimensions, indicating significant roles for arc efficiency and thermal distribution. The plate HAZ showed a clearer positive correlation with HI, whereas the pipe HAZ remained relatively narrow (~1–2 mm) across all conditions, consistent with the asymmetric heat flow and geometric constraints.

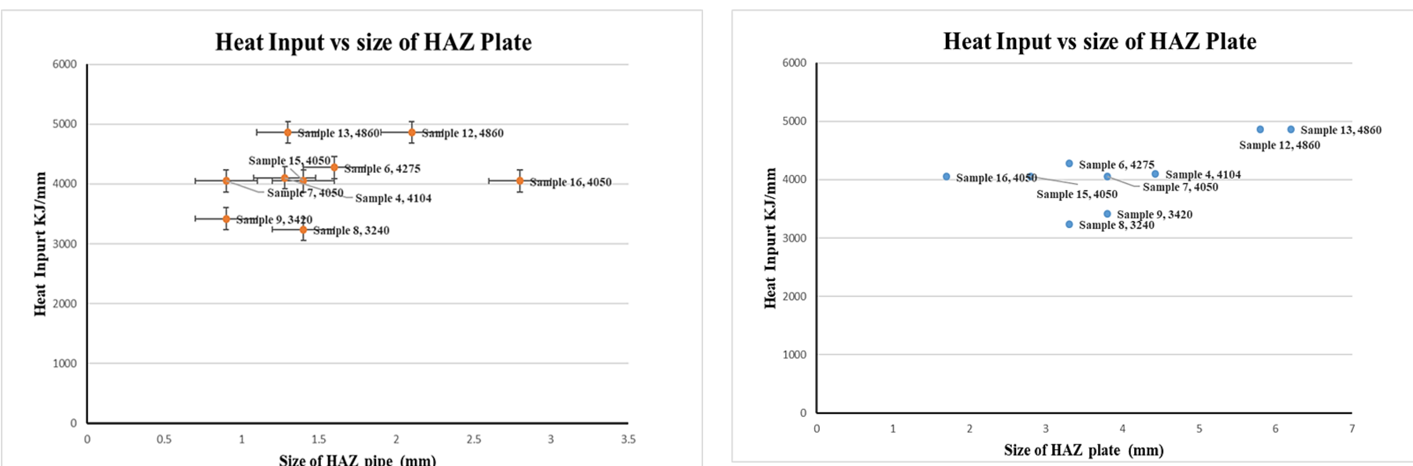

(a) (b)

Figure 3. (a) Diagram of the heat input (HI) values plotted against the size of the HAZ pipe. (b) Diagram of the HI vs HAZ of the plate

4.2 Welding Residual Stresses

As depicted in Figure 5, neutron diffraction measurements consistently showed hoop stress as the dominant residual stress component in both the pipe and flange, surpassing axial and radial stresses. Peak hoop stresses, reaching approximately 425 MPa in the flange and 558 MPa in the pipe, underscore the pipe region's heightened susceptibility to stress accumulation, likely due to multipass thermal cycling and geometric constraints.

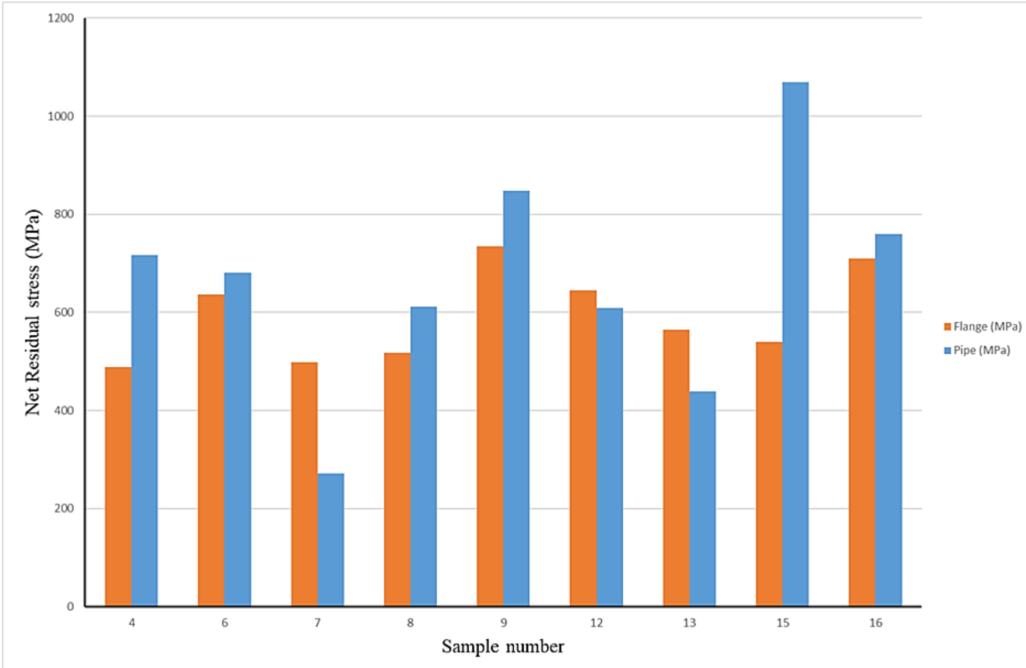

Figure 4. A bar graph of the net welding residual stress measured in the pipe and the plate (flange)

Figure 6 further illustrates the relationship between calculated heat input (HI) and net welding residual stresses (WRS). Samples welded with lower current and voltage combinations consistently exhibited reduced net residual stresses. Changes in welding mode (CA vs. CW) had only a secondary influence on WRS. Importantly, these results demonstrate that a higher HI does not necessarily correlate with higher residual stress. This confirms that residual stress development is governed by a complex interplay of thermal gradients, solid-state phase transformations, and restraint conditions, rather than being solely dependent on heat input.

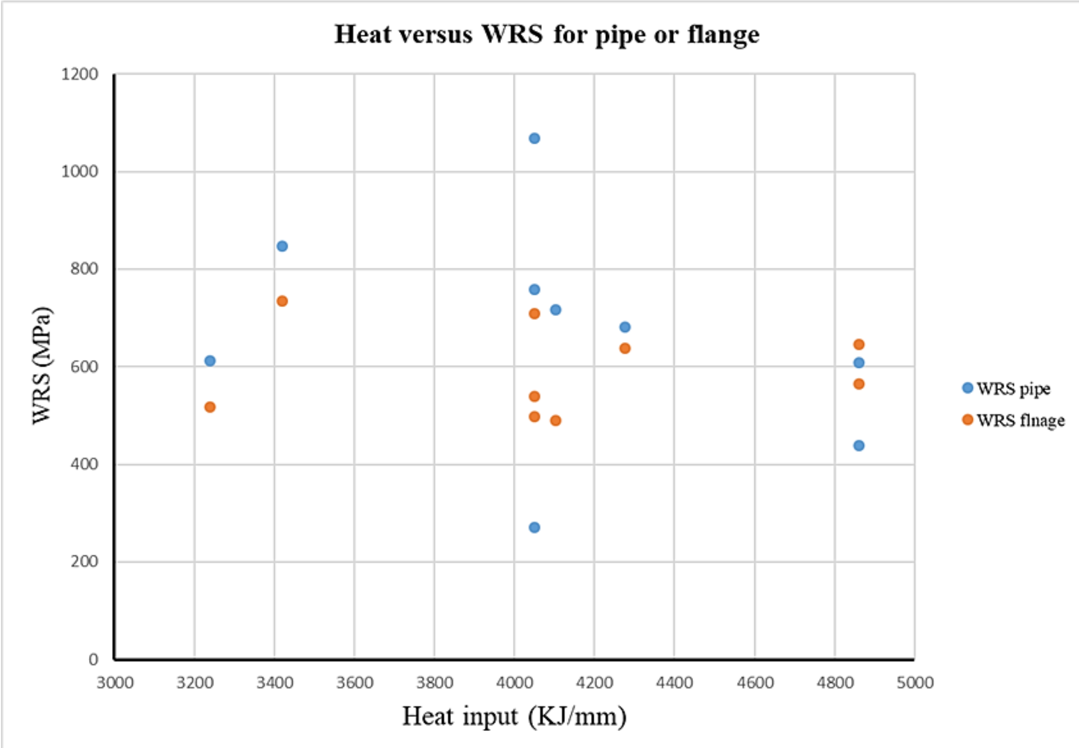

Figure 5. Diagram showing the effect of heat input on the WRS in the flange and in the pipe

4.3 Microstructural Evolution

Figure 7 shows the L-shaped specimen and microstructure in each region. Both the as-received ASTM A516 Gr70 plate and ASTM A106 GrB pipe exhibited typical ferrite–pearlite microstructures. Welding introduces distinct metallurgical zones, including the base metal, HAZ, fusion zone, and weld metal. The weld metal and adjacent HAZ contained martensitic and Widmanstätten ferrite morphologies formed owing to rapid cooling and repeated thermal cycling. Coarse-grained regions near the fusion boundary reflected prolonged exposure to elevated temperatures, whereas subcritical HAZ regions showed refined ferrite–pearlite with tempered martensite, consistent with multipass welding behavior. These distinct microstructural gradients directly underpin the observed variations in hardness and residual stress distributions across the welded joint.

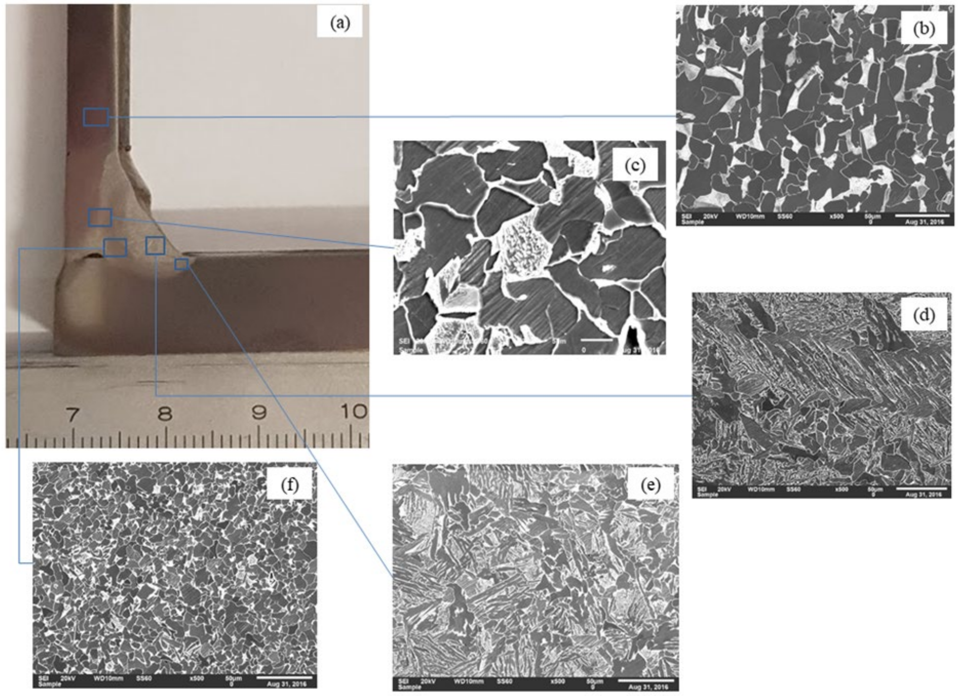

Figure 6. (a) A photograph of the L-shaped welded, polished and etched test specimen showing both the flange and the pipe and the different weld regions. (b) Micrograph of unaffected region in the pipe. (c) Micrograph of the transition zone between the pipe and the heat affected zone. (d) Micrograph of the weld. (e) Micrograph of transition from HAZ to weld. (f) Micrograph of the HAZ pipe

4.4 Phase Analysis (XRD)

As shown in Figure 8, XRD patterns confirmed a body-centered cubic (BCC) ferritic structure in the as-received materials, characterized by dominant {110} reflections. As-welded samples, however, displayed additional peaks corresponding to pseudo-tetragonal martensite, typical of low-carbon steels. Post-weld heat treatment (PWHT) at elevated temperatures reduced the martensitic peak intensity for air- and furnace-cooled samples, indicating phase homogenization, whereas water-quenched specimens retained strong martensitic signatures.

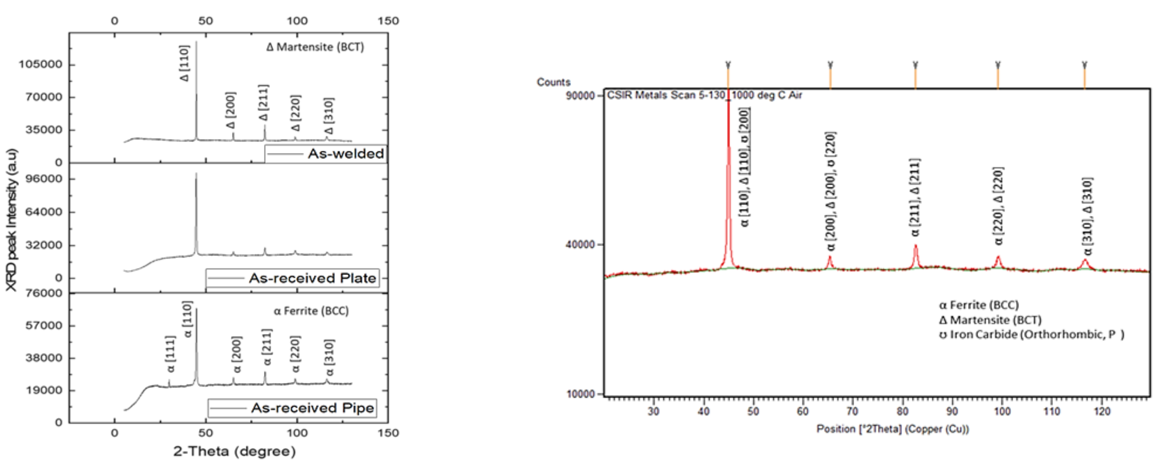

Figure 7. XRD scans of the test specimens as-received of the plate, as-received of the pipe, and the XRD plot of the heat-treated specimen and air-cooled.

4.5 Hardness and Derived Mechanical Properties

Figure 9 illustrates the hardness profiles across the pipe, weld, and flange regions for as-welded and post-weld heat-treated specimens (water-quenched, air-cooled, and furnace-cooled at 950°C and 1050°C). The as-received pipe exhibited a higher hardness (~250 HV) than the plate (~200 HV). The as-welded specimens exhibited pronounced hardness peaks in the weld metal and adjacent HAZ, attributable to martensitic formation and residual stresses. PWHT at 950 and 1050°C with air or furnace cooling significantly reduced the hardness and flattened the hardness gradients, reflecting stress relief and martensite tempering. In contrast, water quenching produced excessive hardness (up to ~490 HV), rendering these conditions unsuitable for pressure vessel application.

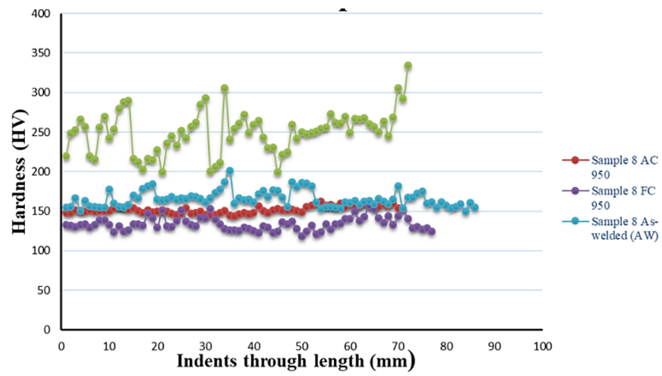

(a)

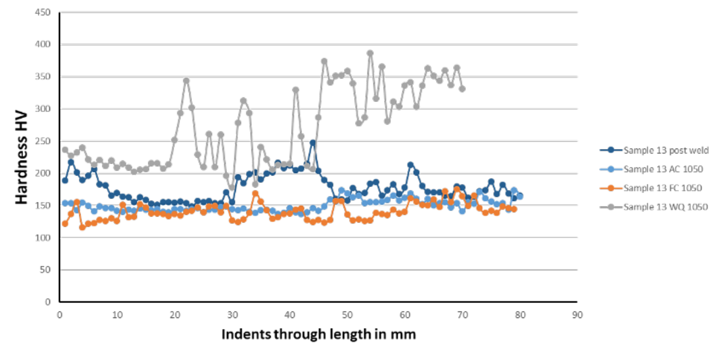

(b)

Figure 8. Welding profile of as-welded specimen compared to PWHT specimen at 950^{o}C and 1050 °C cooled using three different methods.

The mechanical properties derived from the hardness measurements followed similar trends. The as-welded condition yielded the highest estimated tensile strength owing to martensitic strengthening. PWHT at 950°C caused marked softening, whereas treatment at 1050°C enabled partial strength recovery through recrystallization and microstructural homogenization. Furnace and air cooling produced balanced strength levels with improved uniformity, whereas water quenching resulted in brittle and high-strength microstructures.

4.6 Overall Implications

The results demonstrate that the selection of welding parameters significantly influences the heat input, heat-affected zone development, residual stress distribution, and resulting microstructure–property relationships in dissimilar pressure-vessel steel joints. Crucially, while heat input influenced bead geometry and HAZ size, particularly in the plate material, its lack of a direct or linear correlation with welding-induced residual stresses challenges conventional assumptions. This finding underscores that residual stress evolution is dictated by a complex interplay of thermal cycles, phase transformations, and joint geometry, offering a more nuanced understanding vital for predictive modeling and process control.

Residual stresses were consistently higher in the pipe region than in the plate, highlighting the role of geometric constraints and multipass thermal accumulation in the nozzle–shell configurations. Microstructural analysis confirmed that the as-welded joints contained martensitic and Widmanstätten ferrite structures in the weld and HAZ, contributing to elevated hardness and tensile strength, but also increased residual stress levels.

Post-weld heat treatment effectively modified the microstructure and mechanical response of the joints. Air- and furnace-cooled PWHT promoted microstructural homogenization toward ferrite–pearlite morphologies, reduced hardness gradients, and lowered residual stresses, whereas water quenching produced predominantly martensitic structures with excessive hardness and reduced suitability for pressure-vessel service. These findings indicate that controlled cooling after the PWHT is critical for achieving a balanced mechanical performance.

From an engineering perspective, this study provides practical guidance for optimizing welding and post-weld heat treatment strategies for pressure vessel nozzle attachments. From an engineering perspective, these findings provide concrete guidance: employing moderate heat input during SAW and subsequently applying controlled PWHT, specifically normalizing or annealing with air or furnace cooling, presents an optimized pathway. This approach effectively minimizes detrimental tensile residual stress concentrations and homogenizes microstructure, thereby enhancing the structural integrity, fatigue life, and overall service reliability of critical pressure vessel nozzle attachments.

5. Conclusion

This study successfully achieved its objectives by systematically investigating the complex interplay of submerged arc welding (SAW) parameters and post-weld heat treatment (PWHT) on the residual stress state, microstructure, and mechanical properties of dissimilar ASTM A516 Gr.70–ASTM A106 Gr.B pressure-vessel nozzle–shell joints.

The study quantified how welding current, voltage, travel speed, and wire feed rate collectively influence heat input, bead geometry, and HAZ dimensions, revealing a non-monotonic relationship between heat input and residual stress. Although increased heat input generally results in larger HAZ dimensions, particularly in the plate material, no direct or monotonic relationship between heat input and welding-induced residual stress has been observed. Neutron diffraction measurements confirmed that residual stresses, particularly elevated in the pipe region due to geometric constraints and thermal cycling, are governed by a complex interaction of thermal gradients, joint geometry, and phase transformations.

Microstructural characterization revealed distinct metallurgical zones across the welded joint, with martensitic and Widmanstätten ferrite structures forming in the weld metal and adjacent HAZ in the as-welded condition. These microstructures were associated with elevated hardness and tensile strength, as confirmed by Vickers hardness measurements and hardness-derived mechanical-property calculations. X-ray diffraction analysis verified the predominance of body-centered cubic ferrite with martensitic phases in the as-welded specimens.

Post-weld heat treatment was shown to be an effective strategy for tailoring the microstructure and mechanical response of the joints. Air- and furnace-cooled treatments at 950 °C and 1050 °C promoted microstructural homogenization toward ferrite–pearlite morphologies, reduced hardness gradients, and mitigated residual stresses. In contrast, water quenching produces predominantly martensitic structures with excessive hardness, rendering such cooling routes unsuitable for pressure-vessel service.

The unique contribution of this research lies in its integrated approach, combining neutron diffraction, detailed microstructural analysis, and hardness-based mechanical property evaluation to establish robust process–structure–property relationships within a realistic nozzle-to-shell configuration. These findings provide concrete guidance for optimizing SAW parameters and PWHT selection, directly enhancing the structural integrity, reliability, and service life of critical pressure vessel components. Future research should extend this analysis to long-term performance, including fatigue life assessments, and explore advanced PWHT techniques or novel welding strategies to further refine mechanical properties and residual stress management.

References

Abdel-Karim, R., El-Mahallawy, N., Ahmed, H.A., 2018. Corrosion behavior of ASTM A106 Grade B carbon steel in sulfate environments. *Corros. Sci.* 138, 1–10.

Akademia Baru, A., Rahman, M.M., Noor, M.M., 2016. Mechanical and metallurgical properties of ASTM A516 Grade 70 steel for pressure vessel applications. *J. Adv. Res. Appl. Mech.* 24, 1–12.

Akbari, D., Sattari-Far, I., 2009. Effect of welding residual stresses on brittle fracture assessment of pressure vessels. *Int. J. Press. Vessels Pip.* 86, 484–492.

ASME, 2015. *ASME Boiler and Pressure Vessel Code*, Section VIII, Division 1. American Society of Mechanical Engineers, New York.

Croft, T.N., 1989. Submerged arc welding of pressure vessels. *Weld. J.* 68, 45s–52s.

Daavaria, M., Sadough Vanini, S.A., 2016. Mechanical behavior of welded ASTM A106 Grade B steel pipes. *Mater. Des.* 90, 586–594.

De, A., Silva, D.A., 2009. Residual stress development in multipass welded ASTM A516 Grade 70 steel. *J. Mater. Process. Technol.* 209, 5043–5052.

Deng, D., 2009. FEM prediction of welding residual stress and distortion in carbon steel structures. *Comput. Mater. Sci.* 46, 336–347.

Gottlieb, J., 2010. Pressure vessel steels: metallurgical considerations and performance. *Mater. Sci. Technol.* 26, 129–138.

Kou, S., 2002. *Welding Metallurgy*, 2nd ed. Wiley, New York.

Lu, J., 2002. *Handbook of Measurement of Residual Stresses*. Society for Experimental Mechanics, Bethel.

Moradi, M., Salehebrahimnejad, S., 2017. Experimental and numerical investigation of residual stress reduction in PWHT-treated A106 Gr B welds. *Int. J. Press. Vessels Pip.* 153, 1–9.

Oliveira, J.P., Miranda, R.M., Fernandes, F.M.B., 2009. Residual stresses and hardness in multipass welds of ASTM A516 Grade 70 steel. *Mater. Des.* 30, 3743–3751.

Pavlina, E.J., Van Tyne, C.J., 2008. Correlation of yield strength and tensile strength with hardness for steels. *J. Mater. Eng. Perform.* 17, 888–893.

Qin, Y., Wu, Y., Li, X., 2018. Influence of post-weld heat treatment on residual stress and microstructure in carbon steel welds. *Mater. Sci. Eng. A* 712, 664–672.

Rossini, N.S., Dassisti, M., Benyounis, K.Y., Olabi, A.G., 2014. Methods of measuring residual stresses in components. *Mater. Des.* 35, 572–588.

Sharma, S., Singh, R., 2020. Effect of strain rate on fracture toughness of ASTM A516 Grade 70 steel. *Eng. Fract. Mech.* 228, 106896.

Suryana, D., Nugroho, S., Suprapto, W., 2019. Effect of submerged arc welding parameters on bead geometry and HAZ characteristics. *J. Manuf. Process.* 45, 682–690.

Tirenti, M., 2024. Design and integrity assessment of pressure vessels. *Int. J. Press. Vessels Pip.* 211, 105029.

Wang, X., Liu, Z., Zhang, Y., 2024. Effect of post-weld annealing on microstructure and toughness of SA516 Grade 70 steel joints. *Mater. Sci. Eng. A* 890, 146034.

Yingsamphancharoen, T., Sangsawang, P., 2016. Effect of welding current on corrosion behavior of ASTM A106 Grade B steel. *Anti-Corros. Methods Mater.* 63, 307–315.

Biographies

Lerato Shoke is a qualified metallurgical engineering technologist with a specialization in materials subjected to blast and ballistic loading conditions. She has recently submitted her Master's degree in Engineering at the University of Johannesburg, South Africa. With over 15 years of experience in defense research, Ms. Shoke has made significant contributions to the advancement of materials performance and protection technologies within the sector.

Dr. Kalenda Mutombo is an experienced Senior Researcher with a demonstrated history of working in industry and research and development. Skilled in Manufacturing processes such as casting, thermomechanical, and additive manufacturing, in alloy development and production, and in characterization such as Scanning Electron Microscopy, Finite Element Analysis, and Failure Analysis. Strong research professional with a Doctor of Philosophy (PhD) in Physical Metallurgy from the University of Pretoria/Universiteit van Pretoria.

Prof Peter Olubambi is an academic researcher from University of Johannesburg. The author has contributed to research on the following topics: spark plasma sintering and microstructure. The author has an h-index of 28 and has co-authored 305 publications. The previous affiliations of Peter Apata Olubambi include the Federal University of Technology Akure and the University of Manchester.

Dr. Mthobisi Zondi is an experienced executive and engineer with a career spanning over 25 years in the defense, logistics, energy, and public sectors. He is currently the Executive Chair of Sandock Austral Defence, Chair of the LogiDist Group, and Chair of PalletBiz SADC. His career includes 12 years in the South African Department of Defence, where he was the Chief Defence Material Officer. He also held executive roles at PetroSA and Transnet and served as the Chairperson of the Future Defence and Innovation Committee of the AMD Board.